

Study of the characteristics of the flow regimes and dynamics of coarse particles in pipeline transportation

Ting, Xiong; Xinzhuo, Zhang; Miedema, Sape A.; Xiuhan, Chen

DOI

[10.1016/j.powtec.2019.02.031](https://doi.org/10.1016/j.powtec.2019.02.031)

Publication date

2019

Document Version

Final published version

Published in

Powder Technology

Citation (APA)

Ting, X., Xinzhuo, Z., Miedema, S. A., & Xiuhan, C. (2019). Study of the characteristics of the flow regimes and dynamics of coarse particles in pipeline transportation. *Powder Technology*, 347, 148-158. <https://doi.org/10.1016/j.powtec.2019.02.031>

Important note

To cite this publication, please use the final published version (if applicable). Please check the document version above.

Copyright

Other than for strictly personal use, it is not permitted to download, forward or distribute the text or part of it, without the consent of the author(s) and/or copyright holder(s), unless the work is under an open content license such as Creative Commons.

Takedown policy

Please contact us and provide details if you believe this document breaches copyrights. We will remove access to the work immediately and investigate your claim.



Study of the characteristics of the flow regimes and dynamics of coarse particles in pipeline transportation

Xiong Ting^{a,b}, Zhang Xinzhuo^a, Sape A. Miedema^b, Chen Xiuhan^{b,*}

^a School of Energy and Power Engineering, Wuhan University of Technology, Wuhan, Hubei 430063, PR China

^b Section Offshore and Dredging Engineering, Delft University of Technology, Mekelweg 2, Delft, the Netherlands

ARTICLE INFO

Article history:

Received 19 July 2018

Received in revised form 21 January 2019

Accepted 20 February 2019

Available online 22 February 2019

Keywords:

Coarse particles

Horizontal hydraulic conveying

CFD-DEM

Concentration distribution

Flow regimes analysis

ABSTRACT

Slurry transport is a very important means of transporting solids through a pipeline. To improve the efficiency of slurry transport, especially in coarse particle transport, which is subject to problems such as strong resistance and easy blockage, more of the internal structure of the flow must be known. Empirical and analytical models are inadequate for this purpose. Therefore, in this study, a coupling mechanism is established between the computational fluid dynamics (CFD) and discrete element method (DEM). The CFD-DEM coupling was applied and research was conducted on the internal flow structure characteristics of microscopic motion and flow transition for coarse particles in a pipeline. The flow-regime transition processes of coarse 10-mm particles were analyzed qualitatively at velocities of $2 \text{ m} \cdot \text{s}^{-1}$, $5 \text{ m} \cdot \text{s}^{-1}$, $8 \text{ m} \cdot \text{s}^{-1}$ and $10 \text{ m} \cdot \text{s}^{-1}$ in a 0.1524-m diameter pipe, and quantitative analyses were performed on both the concentration distribution and the pressure gradient of particles in regimes of fixed bed flow, sliding bed flow and heterogeneous flow. Moreover, from the perspective of force analysis of particles, the law of sedimentation movement of particles is discussed, and the reason for the change in concentration distribution is explained. The research presented here provides insight into the internal structure of the flow and gives quantitative indications of pressure gradient and concentration distributions.

© 2019 The Authors. Published by Elsevier B.V. This is an open access article under the CC BY-NC-ND license (<http://creativecommons.org/licenses/by-nc-nd/4.0/>).

1. Introduction

Pipeline transportation is a method that uses water as the carrier to transport solid materials through pipes over a long distance and is widely applied because of its advantages of low pollution, energy savings, and high capacity. With the continuous expansion of the application of pipeline transportation, the materials transported have also diversified. Particularly in dredging engineering, dredging objects (not limited to general homogeneous sediment) may include underwater hard rock and soil and may vary in size. Therefore, in pipeline transportation, if the movement characteristics of different particles cannot be determined for selection of the corresponding and suitable transportation conditions, blockage can occur.

Concerning pipeline transportation, Durand & Condolios [2], Jufin & Lopatin (1966), Newitt et al. [4], Wasp et al. (1977), Wilson [10], Doron & Barnea (1987), and Matousek [7], among others, proposed a series of empirical and analytical models and obtained a large number of research results based on the solid-liquid two-phase flow theory and experimental data. The resistance characteristics calculated by these models are often limited to one stable flow regime of particles; however, the flow regime may, in fact, change transiently with the speed,

diameter, or size of particles and many of these models either face a narrow application range or can only be applied to their own test conditions.

Miedema [8,9] divided slurry transport into five flow regimes and integrated five independent models into the DHLLDV framework. This framework also classifies sediment transport into five basic flow regimes, and the complex sediment transport parameters are made dimensionless, achieving comprehensive consideration of the type of energy loss and the role of interphase forces along with a better description of the transition from the heterogeneous flow to the homogeneous flow. Therefore, this calculation framework has wide adaptability and can calculate the pipe resistance characteristics of dredged materials under different dredging conditions.

The core of the aforementioned analytical model is to mathematically describe the characteristics of pipeline transportation based on macroscopic experimental phenomena. Because of the simplifications and assumptions, the model has certain limitations in simulating real-time flow characteristics. The calculation results are incomplete, neither comprehensively revealing the regulations in the characteristics of slurries' movement, nor completely reflecting the flow-development process of slurries inside the pipeline, making this approach a black-box method.

With the parallel development of numerical calculation methods and the computational power of computers, numerical simulation has become an independent and effective research tool. Numerical

* Corresponding author.

E-mail address: X.Chen-1@tudelft.nl (C. Xiuhan).

simulation, if well validated, can replace certain experiments, thus greatly reducing the experimental workload and shortening the experimental period while providing detailed information that experimental methods cannot obtain; as a result, numerical simulation is receiving increasing attention. Two different treatments have been developed for solid particles in a solid-liquid two-phase flow. One treatment is the method that considers the solid particles as a quasi-continuous medium using the representative Euler-Euler model. This method is widely used for the study of pipeline hydraulic transportation. Ekambara [5] used ANSYS-CFX to simulate the horizontal pipeline slurry transportation on the theoretical basis of particle flow dynamics. The simulation results are consistent with the experimental data but are limited to the transport of fine-grained slurry. Kaushal [6] used the Eulerian-Eulerian model to simulate the flow of pipe slurry containing highly concentrated and dispersed particles. They accurately predicted the pressure drop and concentration distribution of the continuous phase; however, they did not capture the flow of individual particles. In short, the method based on the Eulerian model can accurately capture the flow conditions in the entire watershed; however, it cannot accurately describe the interaction between the particles and the liquid phase or the flow characteristics of the discrete particles.

The other treatment, based on the Euler-Lagrangian approach, requires more computational power; this method tracks individual particles and simulates the dynamic behavior of particles in the pipeline. In recent years, this method has been studied by several scholars. Capecelatro & Desjardins [1] used the Euler-Lagrangian model to simulate liquid-solid slurries with an average particle size of 165 μm (particle size range 50–307 μm) in horizontal tubes and studied the kinetic characteristics of the flow at and above the critical settling velocity; they also compared the particle curves of the average volume fraction distribution and velocity distribution with experimental data to verify the accuracy of the simulation. Through high-order statistical analysis, the flow field was found to have three areas below the critical flow velocity: fixed bed, high-friction slip area, and suspended area. The particles showed obvious isolation, with the smallest particles at the top and the largest particles at the fixed bed surface. Through the analysis of forces acting on a single particle, the drag force was found to contribute most to the particle movement. Liu [12] carried out the experiments and the CFD-DEM coupling method to study the two-phase flow of product oil and impurity particles in a pipeline and considered the parameters (such as flow velocity, inclination and diameter of the pipeline, and impurity shape) that may cause changes in the deposition characteristics of the impurity particles. Zhang [11], adopting DEM to describe particle trajectories and interactions between particles and using a density-based buoyancy model to calculate the interaction forces between liquid and solid phases, studied how particles distribute in elbows as the direction of gravity changes and described how the particle-wall interaction force is related to the wear of the wall surface.

In view of the aforementioned analyses, different theoretical models and methods are often used for different transport media. The choice of which method to study depends mainly on the properties of the medium, the size of the medium, and the flow regime of the medium. Hence, in this study, based on the different flow regimes of the slurry transported in the pipeline, appropriate numerical methods were selected to analyze the characteristics of the pipeline transportation resistance and the dynamic characteristics of particles.

2. Analysis of the pipeline flow regime

2.1. Classification of the basic flow regime

Particle flow conditions are generally classified into the following five types: 1) fixed-bed regime or restricted-pipe regime, 2) sliding-bed regime or sliding-friction-dominated regime, 3) heterogeneous-transport or collision-dominated regime, 4) homogeneous transport, and 5) the sliding-flow regime. This study mainly focused on the movement of coarse particles in the pipeline and considered three flow

regimes of coarse particles, namely, fixed-bed flow, sliding-bed flow, and the sliding-flow regime.

The main behavior in the fixed-bed regime is that the solid particles form a stationary bed of particles at the bottom of the pipe such that the fluid can only flow through the confined space above the particle bed; however, under this flow regime, the particles continue to deposit at the bottom of the tube, leading to blockage. With increasing line speed, the fixed bed at the bottom of the pipeline begins to slide and converts to sliding-bed flow, also known as the sliding-friction-dominated flow regime. In this regime, solid particles accumulate at the bottom of pipes to form a layer of continuous forward-sliding particle bed, and a large number of particles flow as a whole solid bed. With increasing line speed, the porosity of the bed increases. At porosities greater than approximately 50%, it is no longer a bed. This situation is called the sliding flow. The flow regime of the sliding bed appears after the fixed-bed flow regime, followed by the sliding flow.

2.2. Identification of the flow regime change

The aforementioned analysis shows that the terminal settling velocity is the key criterion for the particle flow transition. In the transition from the fixed-bed flow to the sliding-bed flow, although the particle remains in the settlement state, the form of movement changes. The transition speed at this time is called the limit of the stationary deposit velocity (LSDV). This change will only occur above a certain particle diameter, a certain diameter ratio and a certain concentration, and only in the case of coarse particles. The formula for the LSDV, after several revisions by Miedema [9], is

$$V_{ls,fs}^2 = \frac{2 \times \mu_{sf} \times g \times C_{vs} \times R_{sd}}{\frac{\lambda_r}{D_H} \times \left(\frac{A_p}{A_H}\right)^2 - \frac{\lambda_l}{D_p}} \quad (1)$$

where A_p is the pipe cross-sectional area, A_H is the cross-sectional area of the restricted region above the particle bed, μ_{sf} is the sliding friction coefficient, C_{vs} is the spatial volumetric concentration, R_{sd} is the relative submerged density, λ_r is the Darcy-Weisbach friction coefficient above the particle-bed limited area, λ_l is the Darcy-Weisbach friction coefficient between the liquid and the pipe wall, D_H is the hydraulic diameter cross section above the particle bed, and D_p is the pipe diameter.

When there is a sliding bed, some particles are suspended above the sliding bed. With increasing line speed, more particles are suspended, but the interaction between the suspended particles and the in-the-bed particles remains a particle-to-particle interaction because the sliding bed still carries the weight of all of the suspended particles, and the weight leads to sliding friction. When the cross-sectional average velocity increases to a certain extent, all the particles will be in a suspended state, and the moving bed flow will change into heterogeneous flow for particles below a certain diameter. At this time, the particles interact with the pipe wall through collision instead of through sliding friction. The limit deposit velocity (LDV) is

$$V_{ls,ldv}^2 = \frac{v_t \times \left(1 - \frac{C_{vs}}{\kappa_c}\right)^\beta \times V_{ls,ldv} + \frac{8.5^2}{\lambda_l} \left(\frac{v_t}{\sqrt{g \cdot d}}\right)^{10/3} \cdot (v_t \cdot g)^{2/3}}{\mu_{sf}} \quad (2)$$

where v_t is the particle terminal settling velocity, κ_c is the concentration eccentricity constant, v_l is the liquid kinematic viscosity, and d is the particle diameter.

For fine and medium-sized particles, a transition occurs from a sliding bed to heterogeneous transport at a certain line speed. For large particles, however, the turbulence is not capable of sufficiently lifting the particles, resulting in a form of sliding-bed behavior above this transition line speed and a possible transition from a sliding-bed regime to a sliding-flow regime when the two conditions described below are met.

One condition for sliding flow regime is that the largest eddies are not large enough in comparison to the size of the particles, and Sellgren & Wilson (2007) used the criterion $d/D_p > 0.015$ for this condition to occur. Another condition is that the concentration of particles is higher than the critical value. Zandi & Govatos (1967) used a factor $N < 40$ as a criterion, with the condition of $N = 2.37/Cvt < 40$ or $Cvt > 0.059$ for sliding flow to occur. This criterion is apparently based on the thickness of sheet flow. If the bed is so thin that the whole bed undergoes sheet flow, sliding flow will not occur; rather, more heterogeneous behavior occurs. If the spatial volumetric concentration is greater than approximately 0.059, then the turbulence is no longer capable of carrying the particles. In this situation, the particles are more likely to settle than to suspend. This condition will result in a high-speed flow with the characteristics of sliding friction; that is, a sliding flow regime appears. Under the condition of sliding-flow regime, the LDV has no physical meaning; thus, it is renamed SBFTV (i.e., the transition velocity from the sliding-bed regime to the sliding-flow regime).

3. Mathematical model

To accurately reflect the dynamic characteristics of slurries and the flow-regime transition, we used the CFD-DEM method to analyze the characteristics of pipeline transportation. The mixture of fine particles and water in the slurries is regarded as a continuum, and the coarse particles carried in the slurries are considered as discrete phases. Suitable particle collision models are selected for different-shaped coarse particles to simulate the motion characteristics of suspended particles in suspension, settling, rolling, etc. In terms of different velocities, concentrations, and sizes of particles, the concentration distribution, velocity distribution, and settling characteristics of the particles are identified at the pipe cross section to reveal the law of changes in resistance characteristics.

DEM is based on Newton's law of motion and combines different constitutive relations (stress-strain relations). The particle system behavior is described by continuously updating the information of the position and velocity through the kinematics and kinetic equations (collision forces and field forces) of each particle in the system. With the interaction between the particles in the two-phase flow taken into consideration, the microscopic characteristics of the particles, such as their particle shape, particle size distribution, collision, and trajectory, can be simulated in detail. The basic idea of the CFD-DEM coupling method is as follows: CFD is used to solve the flow field; DEM is used to calculate the motion of the particle system; and through certain governing equations, these two models can exchange information with each other, e.g., mass, momentum and energy.

3.1. Fluid-phase control equation

In the CFD simulation, the governing equations of particle-free liquid-phase flow used in the study include a vector-based mass conservation equation and the momentum conservation equation:

$$\frac{\partial \rho}{\partial t} + \frac{\partial}{\partial x_i} (\rho u_i) = 0 \quad (3)$$

$$\frac{\partial}{\partial t} (\rho u_i) + \frac{\partial}{\partial x_j} (\rho u_j u_i) = -\frac{\partial p}{\partial x_i} + \frac{\partial \tau_{ij}}{\partial x_j} + F_i \quad (4)$$

where ρ is the liquid density, u_i , u_j is the liquid flow velocity ($i, j = 1, 2, 3$), p is the pressure, g is acceleration due to gravity, τ_{ij} is the stress tensor and F_i is the body force. To describe the phenomenon of turbulence, a standard $k - \varepsilon$ turbulence calculation model is used. The transport equation of the model is

$$\frac{\partial (\rho k)}{\partial t} + \frac{\partial (\rho k u_i)}{\partial x_i} = \frac{\partial}{\partial x_j} \left[\left(\mu + \frac{\mu_t}{\sigma_k} \right) \frac{\partial k}{\partial x_j} \right] + G_k + G_b - \rho \varepsilon - Y_M + S_k \quad (5)$$

$$\frac{\partial (\rho \varepsilon)}{\partial t} + \frac{\partial (\rho \varepsilon u_i)}{\partial x_i} = \frac{\partial}{\partial x_j} \left[\left(\mu + \frac{\mu_t}{\sigma_\varepsilon} \right) \frac{\partial \varepsilon}{\partial x_j} \right] + C_{1\varepsilon} \frac{\varepsilon}{k} (G_k + C_{3\varepsilon} G_b) - C_{2\varepsilon} \rho \frac{\varepsilon^2}{k} + S_\varepsilon \quad (6)$$

where $G_k = \mu_t \left(\frac{\partial u_i}{\partial x_j} + \frac{\partial u_j}{\partial x_i} \right) \frac{\partial u_i}{\partial x_j}$, $G_b = \beta g_i \frac{\mu_t}{Pr_t} \frac{\partial T}{\partial x_i}$, $\beta = -\frac{1}{\rho} \frac{\partial \rho}{\partial T}$, $Y_M = 2\rho \varepsilon M_t^2$, $M_t = \sqrt{k/a^2}$, and $a = \sqrt{\gamma RT}$. Parameter G_k is the turbulent kinetic energy due to the average velocity gradient; G_b is the turbulent kinetic energy due to buoyancy; Y_M is the effect of compressible turbulent pulsatile expansion on the total dissipation rate; and $C_{1\varepsilon}$, $C_{2\varepsilon}$, $C_{3\varepsilon}$ are empirical constants. The default values of FLUENT are $C_{1\varepsilon} = 1.44$, $C_{2\varepsilon} = 1.92$, $C_{3\varepsilon} = 0.09$, and σ_k , σ_ε are the Prandtl numbers corresponding to the turbulent kinetic energy and turbulent dissipation rate, with the default FLUENT values $\sigma_k = 1.0$, $\sigma_\varepsilon = 1.3$; Pr_t is the turbulent Prandtl number, with the default of 0.85; g_i is the component of gravity acceleration in direction i ; β is the thermal expansion coefficient; M_t is the turbulent Mach number; and a is the speed of sound.

In the CFD-DEM approach, the solid-phase momentum conservation considering the particle reaction is

$$\frac{\partial}{\partial t} (\rho \xi u_i) + \frac{\partial}{\partial x_j} (\rho \xi u_j u_i) = -\xi \frac{\partial p}{\partial x_i} + \frac{\partial (\xi \tau_{ij})}{\partial x_j} + n_p (F_{drag} + F_{saffman} + F_{Magnus}) + \xi \rho g \quad (7)$$

where ξ is the solid volume fraction, n_p is the number of particles per unit volume, and F_{drag} , $F_{saffman}$, and F_{Magnus} are the drag force, the Saffman lift force, and the Magnus lift force exerted on a particle, respectively.

3.2. Particle-phase control equation

The Euler model is adopted because the turbulent diffusion of the particle phase and the slip of the average time velocity caused by a difference in the initial phase momentum cannot be neglected. Each individual particle is calculated through a softball model, and the model is described by Newton's equations for translational and rotational motions:

$$m_p \frac{dv_p}{dt} = F_{p-w} + F_{p-p} + F_{drag} + F_{saffman} + F_{Magnus} + m_p g \quad (8)$$

$$I_p \frac{d\omega_p}{dt} = M_p \quad (9)$$

where m_p , v_p , I_p and ω_p are the particle mass, translational velocity, moment of inertia and rotational speed, respectively; F_{p-w} and F_{p-p} are the contact force between the particle and the pipe wall and the contact force between particles, respectively; g is the acceleration due to gravity; and M_p is the net torque due to the contact force. The terms in the Eq. (8) are described in detail in Chu [14] and Karimi [13].

3.3. Interfacial forces

In this study, the model of the drag force obtained experimentally by Di Felice (1994) is given as

$$F_d = \frac{1}{8} C_d \rho_f \pi d_p^2 (U^f - U^p) |U^f - U^p| f(e) \quad (10)$$

where ρ_f is the density of the fluid; d_p is the diameter of the solid particles; U^f and U^p are the velocities of the fluid and the solid, respectively; e is the porosity of the particles; C_d is the drag coefficient that is related

to the Reynolds number as follows:

$$C_d = \left(0.63 + \frac{4.8}{\sqrt{Re_p}} \right)^2 \quad (11)$$

$$Re_p = \frac{e\rho_f d_p |U^f - U^p|}{\mu_f} \quad (12)$$

where μ_f is the dynamic viscosity of fluid; $f(e)$ is related to porosity, which is based on the number of solid particles:

$$f(e) = \begin{cases} 1 & \text{single particle} \\ e^{-m} & \text{particles} \end{cases} \quad (13)$$

where e^{-m} represents the correction factor of the porosity change caused by the interaction between particles; this factor is usually expressed in exponential form, and the exponent m is commonly given as

$$m = 3.7 - 0.65 \exp \left[-\frac{(1.5 - \log_{10} Re_p)^2}{2} \right] \quad (14)$$

The Magnus force and the Saffman force are the key parameters in the lift model. The Magnus force is given as

$$F_{LM} = \frac{1}{2} C_{LM} \pi r^2 \rho_g \frac{\omega_r * u_r}{|\omega_r|} \quad (15)$$

where C_{LM} is the Magnus lift coefficient, r is the solid particle radius, ρ_g is the fluid density, ω_r is the particle rotation velocity, and u_r is the relative fluid velocity.

The Saffman force is as follows:

$$F_{LS} = 6.46 C_{LS} r^2 \sqrt{\rho_g \eta} \frac{u_r D}{\sqrt{D}} \quad (16)$$

where C_{LS} is the Saffman lift coefficient, r is the solid particle radius, ρ_g is the fluid density, η is the fluid viscosity, u_r is the relative fluid velocity, and D is the deformation tensor ratio.

3.4. Wall function

Enhanced wall treatment is used to simulate the flow near the pipe wall. By combining a two-layer model with an enhanced wall function, this method not only features the accuracy of a standard two-layer model in a fine near-wall mesh, but also ensures that the accuracy for the calculation of the wall-function is not significantly reduced.

In this method, the entire area is subdivided into viscosity-affected areas and fully turbulent areas, depending on a wall-based turbulence Reynolds number. In turbulent regions (Reynolds numbers >200), the k- ϵ model or the Reynolds stress model (RSM) are used to solve the problem. In the near-wall region affected by viscosity, a single-equation model by Wolfstein (1969) is used to solve the problem.

3.5. Coupling process

When the CFD-DEM coupling method is used for calculation, the first step is to calculate the flow field in a time step, that is, to solve the original flow field of a continuous phase. The obtained flow field information is passed through the drag-force model (the drag force obtained experimentally by Di Felice) and the lift-force model (Magnus force and Saffman force). Next, the forces are converted into the fluid drag acting on the sand, and then the iterative calculation starts. After the iteration reaches the convergence criterion or the specified number of iteration steps, the calculated flow field data is transferred through the UDF and API interfaces to the EDEM. Meanwhile, based on the flow field data and taking into consideration both the particle collision

information and the interaction force between the particles and the fluid, the EDEM software calculates the force of the particles to obtain their positions. The updated information regarding the particle positions, motion trajectories and velocities is fed back to FLUENT, and then a new round of the coupled calculation process is started.

4. Numerical solution

In this study, the pipe diameter D in the model is 152.4 mm and the length of straight pipe is 7.5 m. The grids of solid and liquid phases are divided respectively. There are 646,720 grids in the whole fluid calculation domain. The mesh is O-shaped, and the height of the mesh's first layer near wall is small enough to achieve the goal of $y^+ < 1$, and the boundary layer is arranged with 20 nodes with a growth rate of 1.2. The ideal particle mesh size is twice the minimum particle radius, but the number of mesh cells is so large that computer memory becomes insufficient. In this case, specifying a 3 times mesh size can reduce the memory usage under the premise of ensuring the accurate calculation. The representation of volume provided by the EDEM Coupling Interface is based on multiple sample points, generated using the Monte Carlo method. EDEM takes regular sample points within the bounding box of a particle and keeps the points that lie within the particles bounding surfaces. Each point is checked to determine which CFD mesh cell it lies within. Sample points are generated for each of the particle types defined in the simulation. Using the position, orientation and scaling of the individual particles, the precise co-ordinates for the points representing each particle can be calculated. The process of using grids in CFD-DEM coupling calculation is shown as Fig. 1.

The fluid phase is set as water, the particle phase is set as sand, the diameter of each sand particle is 10 mm, and the original volume fraction of the solid-phase particle is maintained at 10%. The velocity is set at $2 \text{ m}\cdot\text{s}^{-1}$, $5 \text{ m}\cdot\text{s}^{-1}$, $8 \text{ m}\cdot\text{s}^{-1}$ and $10 \text{ m}\cdot\text{s}^{-1}$ to determine the changes in the flow regime and concentration of slurries at different velocities. The turbulence intensity I is 5%, the particles are standard spherical and its size are 10 mm, and the volume concentration remains unchanged at 10%. Pressure outlet conditions are used for the overflow and sediment outlet. The pressure is atmospheric pressure, the turbulent intensity of reflux is 5%, and the volume fraction of sand reflux is zero. Table 1 presents the specific value of each characteristic parameter in the numerical simulation.

FLUENT and EDEM software are used to solve the liquid-solid two-phase flow field. The liquid flow field in the pipeline is calculated by the FLUENT software, and the k-epsilon turbulence model is selected. When the k-epsilon model works together with the enhanced wall function, the flow field near the wall can be accurately calculated and computer memory could be much released. Such method does not depend on the wall rule, and is suitable for complex flow, especially for low Reynolds number flow, but the mesh is required to be dense, and y^+ should be close to 1. The grids in this paper meet these requirements.

Euler coordinates are used to analyze the movement and distribution of particles in the pipeline. First, the original fluid field results are obtained from FLUENT, and the flow field parameters are passed to the EDEM. The force of the particles under the flow field is calculated by the DEM model in the EDEM, and then the motion parameter of the particles in the next time step is calculated through the internal iteration. At the same time, the particle trajectory is updated. Finally, the EDEM calculation result is returned to FLUENT for the next time step iteration.

5. Results and discussion

In this study, the velocity as the key research variable is set differently to explore how the flow regime, the chord averaged concentration distribution and the pressure gradient change.

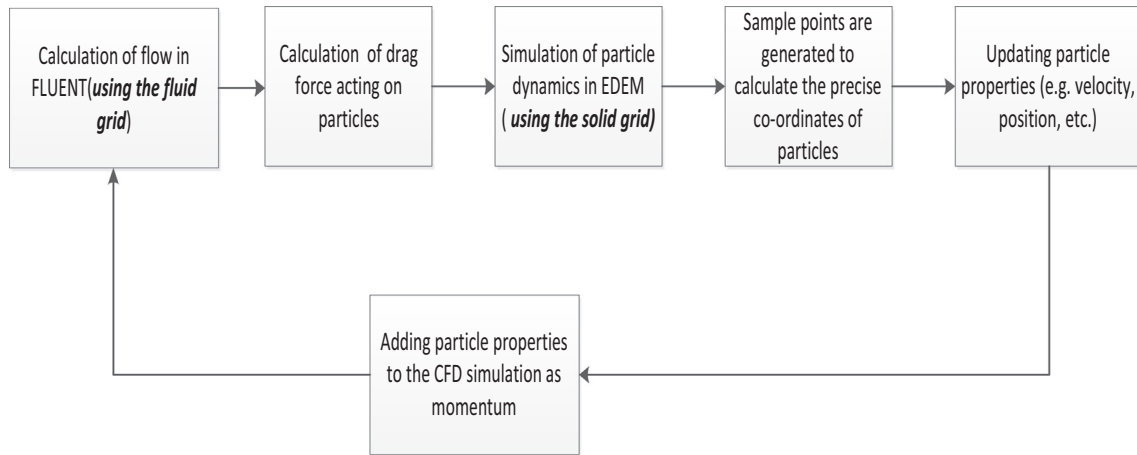


Fig. 1. The process of using grids in CFD-DEM coupling calculation.

5.1. Accuracy verification of simulation

To verify the feasibility of the CFD-DEM method, this study first verifies the model with the experimental data of Vlasak [15]. The working parameters are set to be the same (diameter of 0.1 m, particle diameter of 11 mm, and line speed of $4.1 \text{ m}\cdot\text{s}^{-1}$) and the concentration distribution at a certain cross section at different moments are compared with the experimental data shown in Fig. 2. At 5 s and 10 s, the overall cross-section chord averaged concentration distribution is approximately the same, revealing that the regime is fully developed and that the concentration has reached a stable value. As the particles mostly assemble in the middle and lower parts of the pipeline, the chord averaged concentration is linearly distributed in value, whereas the upper concentration is almost zero. Compared with the experimental data, the simulation data show a consistent trend of concentration distribution; however, the concentration

values from the simulation in the upper part of the pipe are slightly smaller than the experimental values, whereas those in the lower part of the pipe are slightly larger.

Slurries in the pipeline have a high flow velocity near the center of the tube but have a low and stable velocity at the flow core. The area is located roughly at the center of the pipe, but slightly above the center in vertical direction because of the particle bed. Near the wall, where there is a high concentration gradient, the interactions between the particles and the wall and between the particles themselves produce high frictional force and therefore strong shear stress and increasing turbulent kinetic energy, inevitably causing the slurry flow near the wall surface to be in an irregular regime. To study the nature of the slurry at such a location, a semi-empirical method is used to calculate the viscous area between the wall surface and the turbulence area. This empirical formula, however, is limited to certain working conditions; therefore, the simulation results at the bottom of the pipeline deviate from the experimental results, as shown in Fig. 2. This deviation will be reduced if this empirical formula is modified based on a large amount of experimental data.

Table 1
Parameters of the model.

Details	Index	Value		
CFD	Fluid/water-liquid	Density [$\text{kg}\cdot\text{m}^{-3}$]	998.2	
		Viscosity [$\text{kg}\cdot\text{m}^{-1}\cdot\text{s}^{-1}$]	0.001003	
	Velocity-inlet	Velocity [$\text{m}\cdot\text{s}^{-1}$]	2,5,8,10	
	Turbulence	Turbulent intensity	5%	
		Turbulent viscosity ratio	10	
	Pressure-outlet	Gauge pressure [Pa]	0	
	Wall	Wall motion	Stationary wall	
		Roughness height [mm]	0	
	DEM	Particles	Roughness constant	0.5
			Poisson's ratio	0.5
Shear modulus [Pa]			$1.00\text{E}+07$	
Density [$\text{kg}\cdot\text{m}^{-3}$]			2650	
Wall		Poisson's ratio	0.25	
		Shear modulus [Pa]	$1.00\text{E}+10$	
Particle-particle		Density [$\text{kg}\cdot\text{m}^{-3}$]	7800	
		Coefficient of restitution	0.8	
		Coefficient of static friction	0.2	
		Coefficient of rolling friction	0.01	
Particle-wall	Interaction contact model	Hertz-Mindlin (no slip)		
	Coefficient of restitution	0.5		
	Coefficient of static friction	0.5		
	Coefficient of rolling friction	0.01		
Particle generation	Interaction contact model	Hertz-Mindlin (no slip)		
	Particle radius [mm]	5		
	Factory type	Dynamic/unlimited number		
	Generation rate [per second]	6968,17,420,27,870,34,840		

5.2. Identification and analysis of granular flow

In this study, the DHLLDV framework is used to identify the scope of flow regimes according to the parameters in Table 1. The critical velocity of the slurry flow from the fixed bed to the sliding bed flow is $1.719 \text{ m}\cdot\text{s}^{-1}$, and the critical velocity from the sliding bed regime to the sliding flow regime is $3.432 \text{ m}\cdot\text{s}^{-1}$. Fig. 3 shows the hydraulic

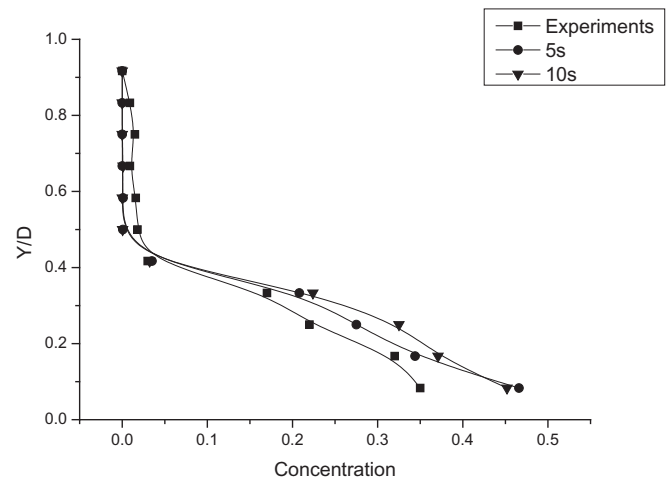


Fig. 2. Experimental data and CFD-DEM simulation data.

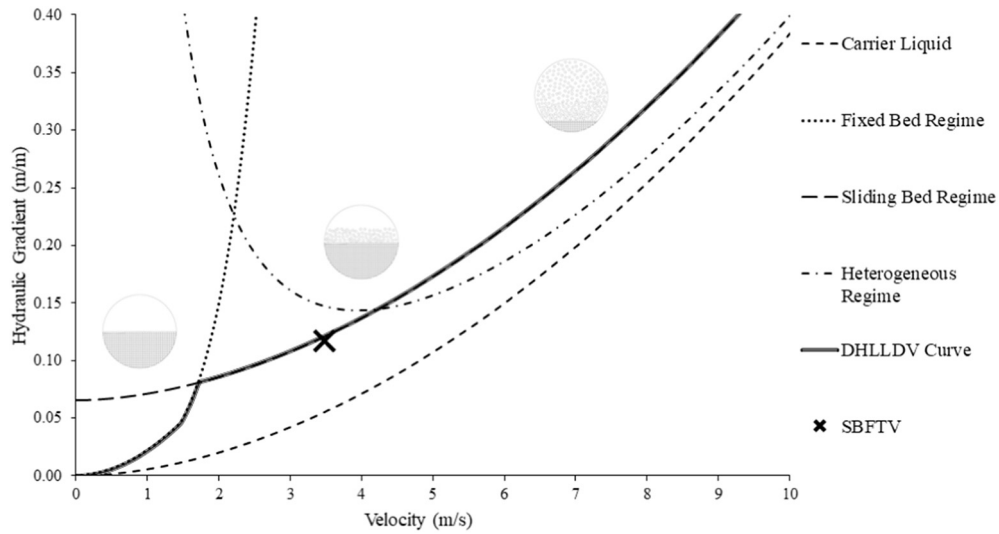


Fig. 3. Hydraulic gradient curve calculated using the DHLLDV model. (a) Incoming flow from the left side of the domain: $V = 2 \text{ m}\cdot\text{s}^{-1}$, fixed bed flow. (b) Incoming flow from the left side of the domain: $V = 5 \text{ m}\cdot\text{s}^{-1}$, sliding bed flow. (c) Incoming flow from the left side of the domain: $V = 8 \text{ m}\cdot\text{s}^{-1}$, sliding flow. (d) Incoming flow from the left side of the domain: $V = 10 \text{ m}\cdot\text{s}^{-1}$, sliding flow.

gradient curves of fixed bed flow, sliding bed flow, and sliding flow. This figure shows the following: when the velocity is lower than LSDV, the particles are in a fixed-bed flow regime; when the particle velocity is higher than LSDV, the bed of particles at the bottom of the pipeline will begin to slide, the particles above the bed will start to slide, roll, or leap, and a turning point will appear in the hydraulic gradient curve; and when the velocity reaches to SBFTV, the sliding bed of particles will be intensely eroded and the regime will convert to the sliding flow regime under the boundary conditions of this study ($d/D_p = 0.066 > 0.015$ and $C_{vt} = 0.1 > 0.059$).

To further analyze the behavior of the particles in the pipe flow, especially the transitions, in this study, four velocities are chosen for the incoming flow, which are $2 \text{ m}\cdot\text{s}^{-1}$, $5 \text{ m}\cdot\text{s}^{-1}$, $8 \text{ m}\cdot\text{s}^{-1}$, and $10 \text{ m}\cdot\text{s}^{-1}$. The flow changes at different velocities are shown in Fig. 4. At a velocity of $2 \text{ m}\cdot\text{s}^{-1}$, the particles cannot be carried by the fluid. A lot of particles

be injected from the inlet into the pipeline. At this moment, the particles, being in a fixed “bed” rapidly settle in the inlet, resulting in that the concentration at the inlet is much higher. Then the drag force generated by the fluid is not enough to push the particles forward and cause a sudden blockage. After that, the velocity of liquid drops sharply and the drag force on the incoming particles also have a huge decrease, so that the blockage is further aggravated, as shown in Fig. 4(a).

When the particles are at a velocity of $5 \text{ m}\cdot\text{s}^{-1}$, they flow in the pipe and the bottom particles will flow as a sliding bed. The particles entering first will continue moving forward and conglomeration reduces. Therefore, the velocity of particles in unrestricted upper area will increase and no blockage happens. However, the granular bed at the bottom of the pipe is unstable, as shown in Fig. 4(b).

When the velocity is increased to $8 \text{ m}\cdot\text{s}^{-1}$, particles remain at the bottom of the pipe; however, the thickness of the granular bed is

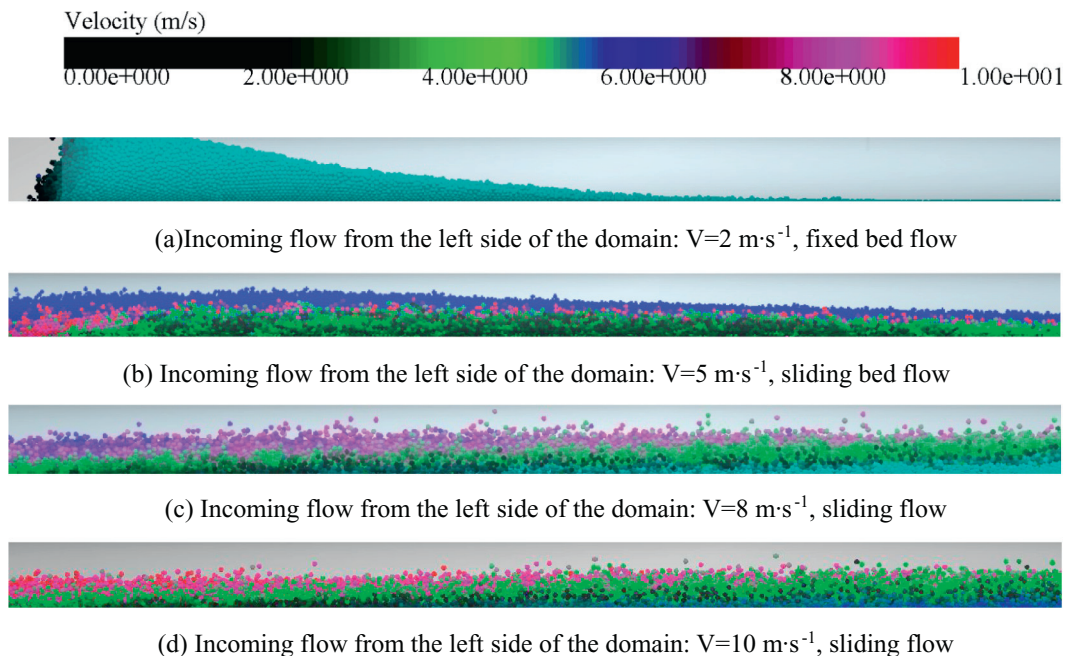


Fig. 4. Analysis of the flow regime at different velocities.

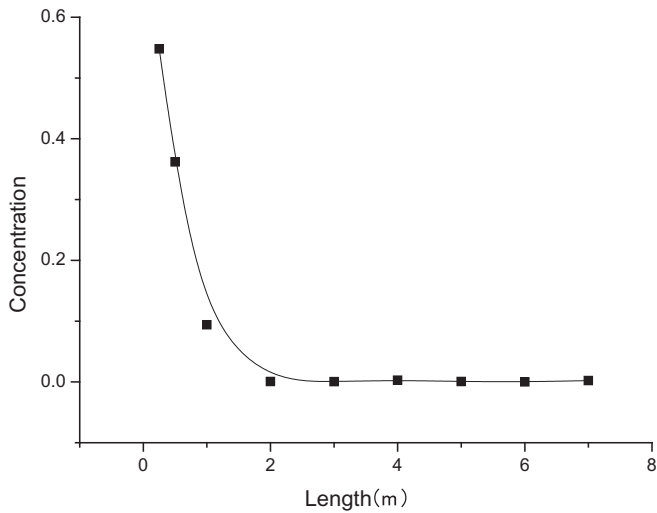


Fig. 5. Slurry concentrations for different times at $2 \text{ m} \cdot \text{s}^{-1}$.

substantially reduced, and the number of particles in the upper part of the pipe obviously increases. Some particles are suspended under the effect of the fluid. Other particles roll and slide at the bottom of the pipe, and the particle flow shows a typical sliding flow regime, as shown in Fig. 4(c). When the velocity increases to $10 \text{ m} \cdot \text{s}^{-1}$, no substantial change is observed in the flow regime; however, the upper part of the pipe has a higher particle velocity, as shown in Fig. 4(d). In Fig. 4(c) and 4(d), the solid phase is found to evolve into the following two regimes: 1) the bottom layer remains in the sliding-bed regime, and 2) the upper layer of the solid phase exhibits a much higher porosity, with each particle being in the sliding-flow regime, with a different set of dominant forces.

The numerical simulation analysis reveals that no clear boundary exists between the flow from the sliding bed to the sliding flow and that the flow regime gradually develops. To further characterize the regime development, we analyzed the concentration distribution.

5.3. Analysis of the concentration distribution

5.3.1. Fixed-bed concentration distribution

At a velocity of $2 \text{ m} \cdot \text{s}^{-1}$, pipes of 0.25 m, 0.5 m, 1 m, 2 m, 3 m, 4 m, 5 m, and 6 m are used to observe the regime development. The chord averaged concentration distribution curve is shown in Fig. 5. The concentration distribution cloud in Fig. 6 shows that great differences exist among the internal concentrations at different pipe locations. Because of the low flow velocity of particles, the fixed-bed flow is formed at the bottom of the pipe; with the continuous addition of particles, the

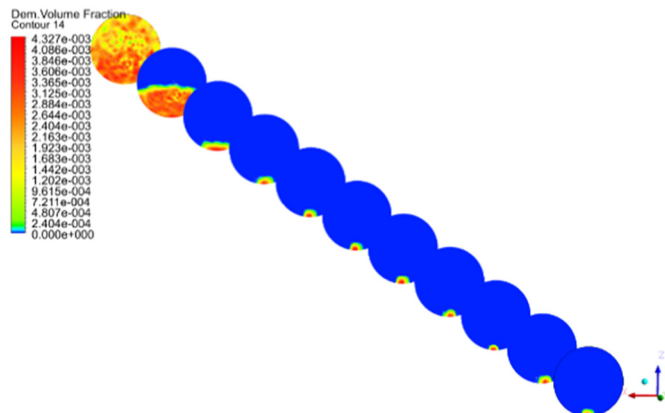


Fig. 6. Concentration distributions for different cross sections at $5 \text{ m} \cdot \text{s}^{-1}$.

pipe blockage obviously occurs at the front 0.5 m of the pipe. After the blockage occurs, the particles cover the entire cross section and the concentration values are almost the same everywhere. In the downstream of the blockage, except for a few particles at the bottom, the concentration is almost zero.

5.3.2. Concentration distribution of the sliding bed

When the velocity increases to the LSDV, the bed of particles at the bottom of the pipeline begins to erode, the upper particles roll or leap irregularly, and the particle bed slides and forms a forward-moving dune in the pipeline. Fig. 7 shows how the slurry chord averaged concentration at different moments changes with different pipe heights at a velocity of $5 \text{ m} \cdot \text{s}^{-1}$. At an initial velocity of $5 \text{ m} \cdot \text{s}^{-1}$, the concentration does not substantially change at either 5 s or 10 s; in contrast, a large difference is observed at 1 s. Therefore, the flow is not fully developed at the moment of 1 s and the concentration at this time remains in an unstable state. Regarding the particle motion characteristics of moving-bed flow, a two-layer model is typically used [3]. The particle suspension of the upper layer is speculated to mainly cause turbulent diffusion; the particle concentration in this layer is usually considered to be so low that their mutual interactions should be ignored. The particles in the lower layer are mainly subjected to sliding friction between the particles and the tube wall. Fig. 7 also reveals that a transition zone known as the shear layer exists in the middle of the pipe between the sliding bed and the suspension zone. The particle concentration in the upper part tends to be zero, whereas that in the lower part tends to be similar to the concentration in the particle bed. Therefore, the concentration of the shear layer is characterized by a high concentration gradient and the collision between the particles in the shear layer dominates the particle movements. From the concentration distribution chart in Fig. 8, the following observations are made: 1) the particle concentration in the uppermost layer is basically zero; 2) the concentration in the middle shear layer ($0.6 \leq Y/D \leq 0.8$) is linearly distributed, and decreases as the height increases, and has a high concentration gradient; and 3) the concentration in the particle bed is the highest and tends to be constant, maintaining a value of approximately 55%.

5.3.3. Concentration distribution of sliding flow

When the velocity is further increased, the flow of the sliding bed gradually changes to a sliding-flow regime. With increasing velocity, the thickness of the sliding bed decreases and particle saltation becomes the dominant mode of particle movement. However, most particles remain in contact with the pipe wall.

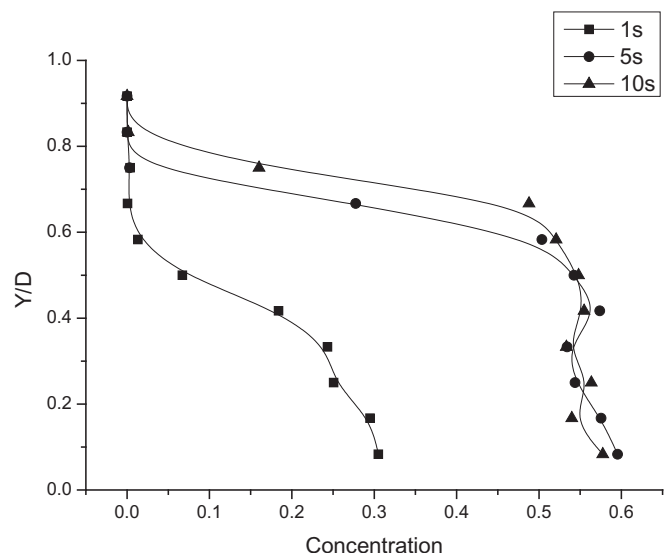


Fig. 7. Slurry concentrations for different times at $5 \text{ m} \cdot \text{s}^{-1}$.

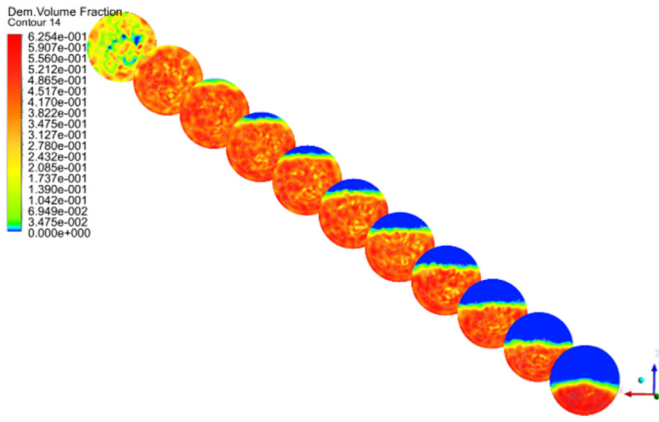


Fig. 8. Concentration distributions for different cross sections at 5 m·s⁻¹.

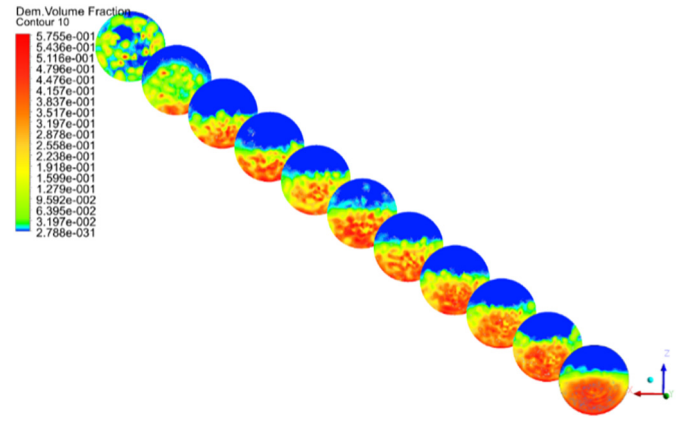


Fig. 10. Concentration distributions for different cross sections at 8 m·s⁻¹.

The curves in Fig. 9 and Fig. 11 show that, at the velocities of 8 m·s⁻¹ and 10 m·s⁻¹, the chord averaged concentration profiles do not show much difference at the time 1 s, 5 s, and 10 s; thus, at these three moments, the slurries are fully developed and reach a stable concentration. For the initial velocities of 8 m·s⁻¹ and 10 m·s⁻¹, the particle concentration in the pipeline no longer exhibits an obvious stratification; rather, it has a linear distribution in the vertical direction and the thickness at the bottom bed decreases. Fig. 10 and Fig. 12 clearly show that, compared with the working condition of 5 m·s⁻¹, those of 8 m·s⁻¹ and 10 m·s⁻¹ have lower particle concentrations in the lower part of the pipeline and more uniform concentration distributions.

5.4. Analysis of the particle force

The change of coarse particle movement in the pipe is the main contributor to the aforementioned flow-regime conversion. When moving, the particles in the slurries are likely to be affected by various forces, such as forces among particles, forces between the particles and the pipe wall, and forces between the solid and liquid phases. Fig. 13 shows the changes of various interactive forces in the slurries at the delivery time of 10 s. In the legend, the compressive force p-p represents the sum of the surface normal forces between particles. The compressive force p-w represents the sum of normal forces from the particles on the pipe's inner surface, and the coupling force p-l represents the force from the fluid phase acting on the particles.

The Y-axis is a dimensionless number (the ratio of each force to the total force) that measures the dominant action of various forces. The force between the particles and the particles is selected based on all the particles in the computational domain and the dimensionless number is used to study the types of dominant force at different conveying velocities. When the conveying velocity is low, the particles into the pipe settle at the bottom of the pipe and start piling up. The drag provided by the fluid is not enough to lift the sediment, so the compressive force (p-p) of the particles plays a leading role. But when the conveying velocity increases, the coupling force of the fluid to the particles also increases, the particle bed is eroded, and the particles gradually change from the sedimentary state to the suspended state. At this time, the dominant force is not solely the compressive force (p-p), and both the compressive force (p-p) and the coupling force (p-l) exert significant influence. If the particle collision is intense, the compressive force (p-p) is slightly larger. If the suspended particles increase, the coupling force (p-l) is slightly larger. The motion state of the particles is affected by two forces.

Fig. 14 shows how three different forces tend to change with time at a line speed of 8 m·s⁻¹. In the initial stage of regime development, new particles, after entering into the pipe, go through the frequent processes of colliding, settling, piling and reactivating, exhibiting an unstable flow regime. The coupled fluid force and the compressive force between the particles gradually increase and reach their maximum values at 5 s. When the flow regime fully develops, particles receive forces that

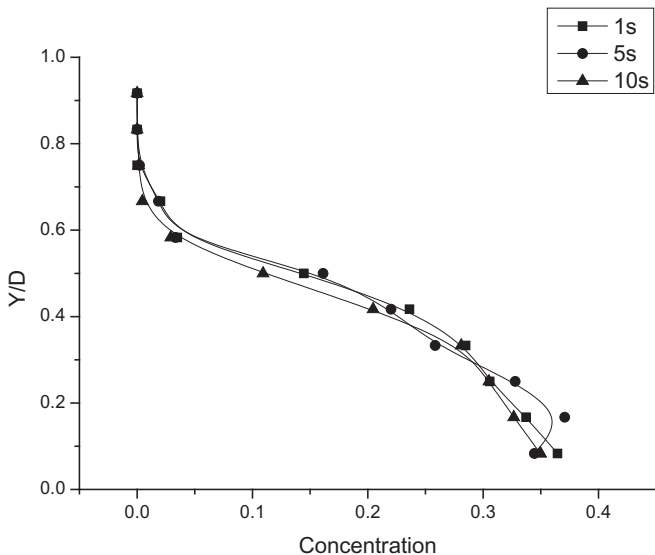


Fig. 9. Slurry concentrations for different times at 8 m·s⁻¹.

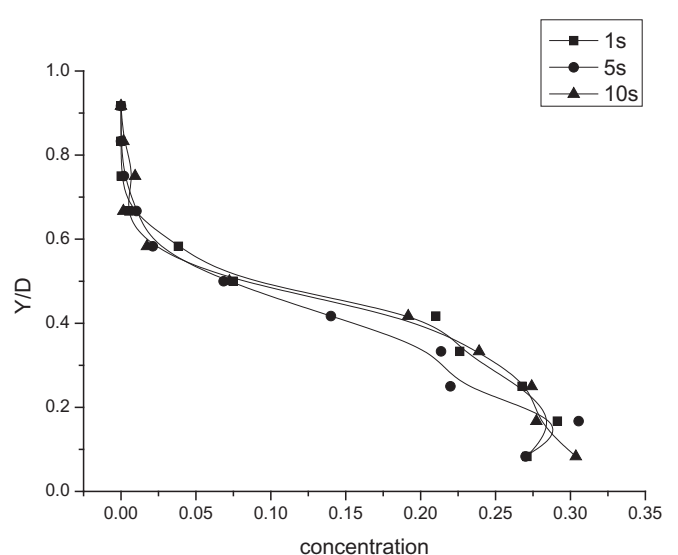


Fig. 11. The slurry concentrations for different times at 10 m·s⁻¹.

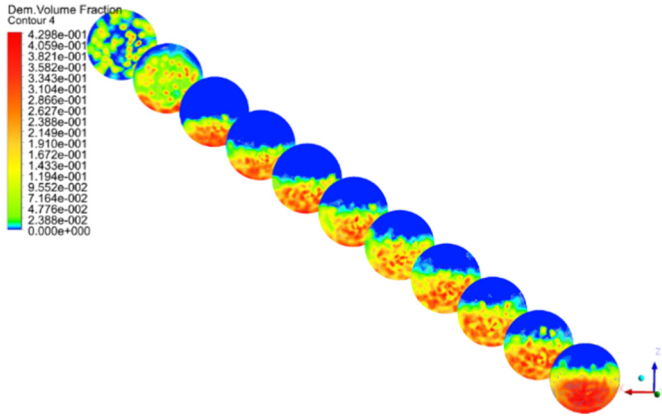


Fig. 12. Concentration distributions for different cross sections at 10 m·s⁻¹.

reduce to a relatively steady value; consequently, a stable sliding flow is maintained. In this regime, particle movements are mainly directed by the coupled fluid force and the compressive force between the particles.

5.5. Analysis of particle deposit velocity

To further know the particle movements in the pipe, this paper study the dynamic properties of particles under different flow regimes, and the velocity is the most important factor to the change of flow state. Therefore, we analyzed the relationship between the particle deposition velocity and the slurry flow velocity, with the results shown in Fig. 15.

At a line speed of 2 m·s⁻¹, in the blocked state, particles have the highest deposition velocity. When the pipe is blocked, the newly ingested particles will find difficulty in entering the pipe and will directly fall off from the entrance. The fallen particles are not dragged by the liquid and are in a state of free sedimentation, which increases the average deposit velocity of the particles during the blockage time.

In addition, at speeds of 5 m·s⁻¹, 8 m·s⁻¹ and 10 m·s⁻¹, the deposition velocity increases with increasing line speed because, when the line speed increases, the collision between the particles intensifies and the force of the coupled liquid on the particles decreases. However, because the turbulent dissipation of the fluid is greatly enhanced by the increasing line speed, the effect of the increase of deposition velocity is negligible, and some particles remain in suspension.

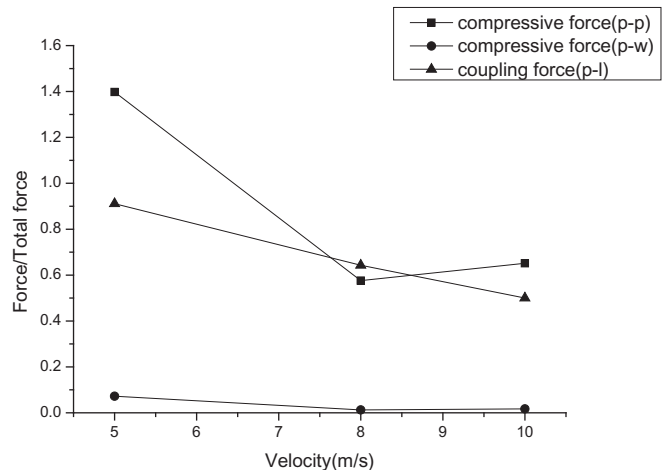


Fig. 13. Change of force for different velocities at 10 s.

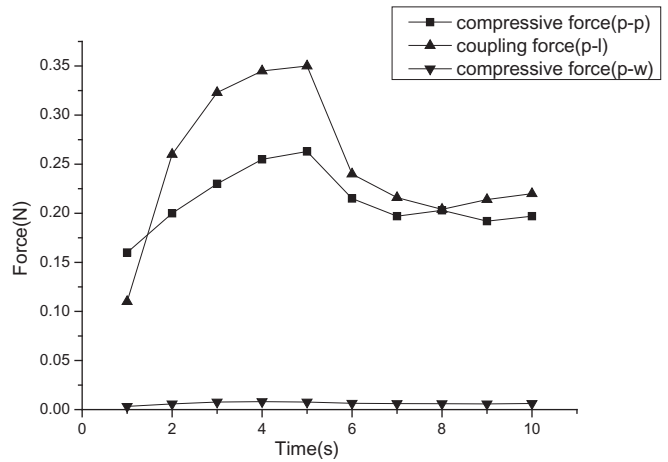


Fig. 14. Change of force versus time at 8 m·s⁻¹.

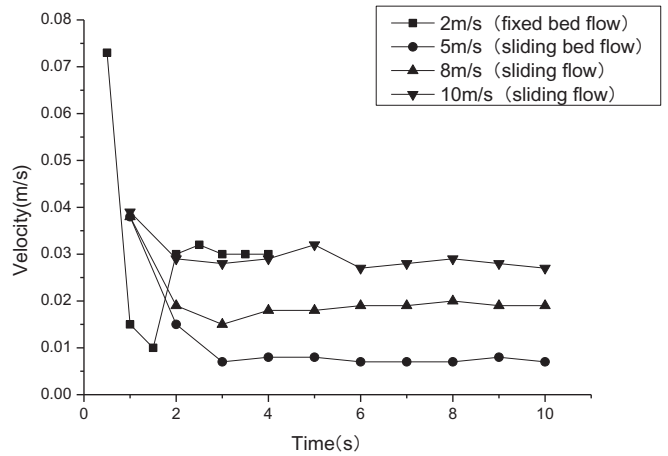


Fig. 15. Deposition velocities at different flow regimes.

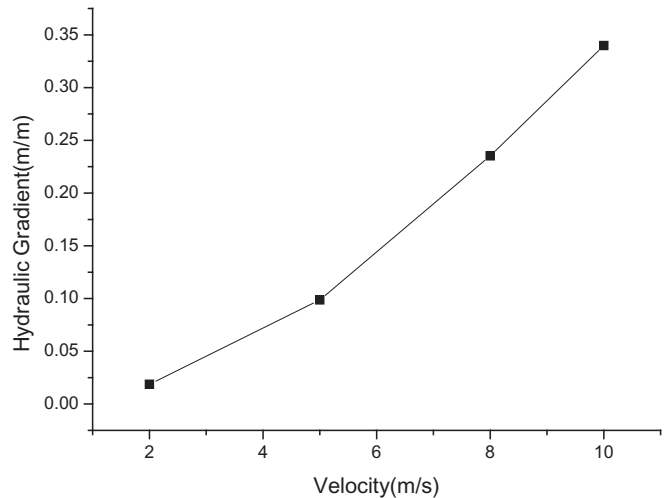


Fig. 16. Pipeline pressure drops at different line velocities.

5.6. Analysis of pressure gradient

There are three causes of resistance loss: resistance loss caused by friction, potential resistance loss caused by particle settling, and resistance loss caused by particle-particle and particle-wall interactions. As

the velocity increases, the flow regimes of the slurries change and the total pressure loss increases, as shown in Fig. 16. However, in different flow regimes, different factors result in pipeline pressure loss: in the fixed-bed flow, the pipeline pressure drop is mainly generated in the confined space on the upper part of the granular bed; in the sliding-bed flow, the pressure drop in the pipeline is caused by the sliding friction from the particles and the viscous friction from the liquid; in the sliding flow, the pressure loss is caused by both sliding friction and particle-particle interaction.

6. Conclusion

The CFD-DEM method was used in this study to analyze the characteristics of coarse particle flow under different velocities. We found that the velocity of coarse particles strongly affects the flow regime of the particles in the pipeline and the distribution of particle chord averaged concentration in the pipeline. The flow characteristics and key influencing factors are summarized as follows:

- 1) At the line speeds of $2 \text{ m}\cdot\text{s}^{-1}$, $5 \text{ m}\cdot\text{s}^{-1}$, $8 \text{ m}\cdot\text{s}^{-1}$ and $10 \text{ m}\cdot\text{s}^{-1}$, the flow regimes are identified through the DHLLDV framework. The results are in agreement with the regime changes simulated by CFD; the regimes are fixed-bed flow, sliding-bed flow and sliding-flow regime flow.
- 2) Fixed-bed flow at $2 \text{ m}\cdot\text{s}^{-1}$ presents an unstable tendency over time. In this case, the continuous accumulation of particles inevitably leads to blockage. Moreover, when blockage occurs, the settling velocity reaches its highest point. Particles in the blocked pipe cover the entire cross section, and the concentrations are basically the same. At the rear of the blocked pipe, the particle concentration in the whole section is almost zero. Few particles are located at the bottom of the pipe.
- 3) Sliding-bed flow at $5 \text{ m}\cdot\text{s}^{-1}$ presents certain changes over time and gradually reaches a stable state. In the initial stage of flow development, particles converge to add to the thickness of the bed. At $5 \text{ m}\cdot\text{s}^{-1}$, the sliding bed will maintain its thickness to move steadily forward after reaching a height of approximately 0.55D and the particle concentration at the top of the pipeline is almost zero.
- 4) Sliding flow is a relatively stable state, where the number of inflow particles is almost equal to the number of outflow particles, with the inner flow stabilizing within a short period and the concentration distributions being similar at 1 s, 5 s, and 10 s. Compared with the sliding-bed flow, a higher concentration in the upper pipe and a lower concentration at the bottom are observed, and no obvious formation of granular bed occurs, with the concentration being nonlinearly distributed in the vertical direction.
- 5) The root cause of the changes in the flow regime is the change in the motion of the particles under different forces. Based on the force analysis of the particles, the interaction between the particles is the main force at any speed. As the line speed rises, the coupling force (p-l) will share the dominance with the compressive force (p-p) because the former dominates force, the compressive force (p-p), decreases.

In summary, the particle flow is the key factor to achieving high efficiency and ensuring the safety of pipeline transportation and an unstable particle bed can cause pipeline blockage. In dredging engineering, for the purpose of achieving lower hydraulic resistance and higher energy efficiency, comprehensive investigation should be made based on the pipe diameter, the particle diameter and the slurry concentrations, only then it is possible to ensure that the velocity offered is in an

appropriate range to keep the particles transported through the pipeline staying in a stable flow regime.

Acknowledgments

The authors are grateful for financial support from the Natural Science Foundation of China (No. 51709210).

References

- [1] J. Capecehatro, O. Desjardins, Eulerian–Lagrangian modeling of turbulent liquid–solid slurries in horizontal pipes[J], Int. J. Multiphase Flow 55 (2013) 64–79.
- [2] R. Durand, E. Condolios, Experimental study of the discharge pipes materiaux especially products of dredging and slurries, Deuxiemes Journees de l'Hydraulique 1952, pp. 27–55.
- [3] P. Doron, D. Barnea, A three-layer model for solid–liquid flow in horizontal pipes, Int. J. Multiphase Flow 19 (6) (1993) 1029–1043.
- [4] D.M. Newitt, M.C. Richardson, M. Abbott, R.B. Turtle, Hydraulic conveying of solids in horizontal pipes, Trans. Inst. Chem. Eng. 33 (1955) 93–110.
- [5] K. Ekambara, R.S. Sanders, K. Nandakumar, et al., Hydrodynamic simulation of horizontal slurry pipeline flow using ANSYS-CFX[J], Ind. Eng. Chem. Res. 48 (17) (2009) 8159–8171.
- [6] D.R. Kaushal, T. Thinglas, Y. Tomita, et al., CFD modeling for pipeline flow of fine particles at high concentration[J], Int. J. Multiphase Flow 43 (2012) 85–100.
- [7] V. Matousek, Pressure drops and flow patterns in sand–mixture pipes[J], Exp. Thermal Fluid Sci. 26 (6–7) (2002) 693–702.
- [8] S.A. Miedema, Slurry Transport Fundamentals, A Historical Overview & The Delft Head Loss & Limit Deposit Velocity Framework, 2017.
- [9] S.A. Miedema, The heterogeneous to homogeneous transition for slurry flow in pipes[J], Ocean Eng. 123 (2016) 422–431.
- [10] K.C. Wilson, Deposition limit nomograms for particles of various densities in pipeline flow. Hydrotransport, vol. 6, BHRA Fluid Engineering, Canterbury, UK 1979, p. 12.
- [11] H. Zhang, Y. Tan, D. Yang, et al., Numerical investigation of the location of maximum erosive wear damage in elbow: effect of slurry velocity, bend orientation and angle of elbow[J], Powder Technol. 217 (3) (2012) 467–476.
- [12] Liu Gang, Tang Yuannan, L.I. Bo, et al., Movement, deposition and influence laws of impurities in the product oil pipelines[J], Oil Gas Storage Transp. 36 (6) (2017) 708–715.
- [13] H. Karimi, A.M. Dehkordi, Prediction of equilibrium mixing state in binary particle spouted beds effects of solids density and diameter differences, gas velocity, and bed aspect ratio[J], Adv. Powder Technol. 26 (2015) 1371–1382.
- [14] K.W. Chu, B. Wang, D.L. Xu, et al., CFD-DEM simulation of the gas–solid flow in a cyclone separator[J], Chem. Eng. Sci. 66 (2011) 834–847.
- [15] P. Vlasak, Z. Chara, J. Krupicka, J. Konfrst, Experimental investigation of coarse particles water mixture flow in horizontal and inclined pipes, J. Hydrol. Hydromech. 62 (3) (2014) 241–247.

Nomenclature

A_p	: Pipe cross-sectional area
C_{VS}	: Spatial volumetric concentration
C_d	: Drag coefficient
C_{LM}	: Magnus lift coefficient
C_{LS}	: Saffman lift coefficient
D_p	: Pipe diameter
d	: Particle diameter
D_H	: Hydraulic diameter
D	: Deformation tensor ratio
F_i	: Body force
F_{drag}	: Drag force
$F_{saffman}$: Saffman lift force
F_{magnus}	: Magnus lift force
G_b	: Turbulent kinetic energy due to buoyancy
G_k	: Turbulent kinetic energy due to the average velocity gradient
κ_c	: Concentration eccentricity constant
g	: Gravitational constant
I_p	: Moment of inertia
M_t	: Turbulent Mach number
M_p	: Net torque due to the contact force
m_p	: Particle mass
ρ	: Density of liquid
λ_p	: Darcy–Weisbach friction coefficient above the particle-bed limited area
λ_L	: Darcy–Weisbach friction coefficient between the liquid and the pipe wall,
τ_{ij}	: Stress tensor
κ_c	: Concentration eccentricity coefficient
β	: Thermal expansion coefficient
n_p	: Number of particles per unit volume
p	: Pressure
Pr_t	: Turbulent Prandtl number
R_{sd}	: Relative submerged density

v_t : Particle terminal settling velocity

ν_l : Liquid kinematic viscosity

v_p : Translational velocity of solid phase

Y_M : Effect of compressible turbulent pulsatile expansion on the total dissipation rate

ξ : Solid volume fraction,

τ_s : Stress-strain tensor of solid phase

e : Porosity of the particles

μ_{sf} : Sliding friction coefficient

ω_p : Rotational speed

σ_k : Prandtl numbers corresponding to the turbulent kinetic energy

σ_ε : Prandtl numbers corresponding to the turbulent dissipation rate

ε : Dissipation rate